# Microscopic three-cluster study of 21-nucleon systems

P. Descouvemont
*Physique Nucléaire Théorique et Physique Mathématique, Université Libre de Bruxelles, Campus Plaine, C.P. 229, B1050 Bruxelles, Belgium*
(Received 1 July 1993)

The three-cluster generator coordinate method is applied to different properties of $T = \frac{1}{2}$ 21-nucleon systems. The $^{21}$Ne and $^{21}$Na nuclei are described by mixing of different $^{16}O+\alpha+n$ or $^{16}O+\alpha+p$ configurations. A fair agreement with experiment is found for energy spectra and for electromagnetic transition probabilities. We present $^{17}O+\alpha$ and $^{20}Ne+n$ elastic phase shifts, as well as $^{17}O(\alpha,\gamma)^{21}Ne$ and $^{17}O(\alpha,n)^{20}Ne$ low-energy cross sections. The ratio between the corresponding reaction rates is predicted 5 orders of magnitude lower than values currently used in astrophysics. We also compare $^{20}Ne(p,p')^{20}Ne(2^+)$, $^{20}Ne(p,\alpha)^{17}F$, and $^{20}Na(p,\gamma)^{21}Na$ theoretical cross sections with experimental data. For the proton capture reaction, important in stellar evolution, we do not suggest significant differences with the existing reaction rate.

PACS number(s): 21.60.Gx, 21.30.+y, 27.30.+t

## I. INTRODUCTION

The structure of the $^{21}$Ne and $^{21}$Na nuclei, as well as reactions involving them, have drawn the attention of many authors [1–7]. However, in spite of these numerous studies, some important uncertainties remain. In $^{21}$Ne, spin assignments are clear up to 5 MeV only, an energy lower than the $^{20}Ne+n$ and $^{17}O+\alpha$ breakup thresholds (6.76 MeV and 7.35 MeV, respectively). A similar situation occurs in $^{21}$Na where even the second excited state does not have a definite spin assignment [7]. Several reactions, involving $^{21}$Ne or $^{21}$Na as a unified nucleus, are relevant for astrophysical applications. Up to now, there is little experimental information on the low-energy $^{17}O(\alpha,n)^{20}Ne$ and $^{17}O(\alpha,\gamma)^{21}Ne$ cross sections. Consequently, the corresponding reaction rates are very uncertain [8]. The situation is slightly different for the $^{20}Ne(p,\gamma)^{21}Na$ cross section, which has been measured by Rolfs *et al.* [6] at energies down to 350 keV. However, the astrophysically important energies are still much lower (typically 100 keV) and a direct measurement is prohibited by the smallness of the cross section. The $^{20}Ne(p,\gamma)^{21}Na$ cross section is expected to be strongly affected by the weakly bound ($-7$ keV) $1/2^+$ bound state in $^{21}$Na. Therefore, the extrapolation of the available data is a tedious task, and requires a theoretical support.

To our knowledge, theoretical approaches to $^{21}$Ne and $^{21}$Na systems are restricted to shell-model studies (see references in Ref. [5]). Consequently, high-energy excited states are not described with a good accuracy since the scattering asymptotic behavior of the wave functions is not taken into account. For the same reason, nonresonant contributions of low-energy cross sections are not accessible.

In the present paper, we aim at investigating the $^{21}$Ne and $^{21}$Na nuclei in a microscopic [9] three-cluster model, involving $^{16}$O, $\alpha$, and $n$ (or $p$) particles. The three-cluster generator coordinate method (GCM) has been recently applied to several systems [10,11]. The model starts from a nucleon-nucleon interaction and basis wave functions suitable for the problem. This gives a predictive power to the GCM since, once the nucleon-nucleon interaction is chosen, there is no more adjustable parameter. In addition, bound, resonant, and scattering states of a system are described in an unified way. This enables one to test the model with well known experimental data and to calculate unknown quantities, such as low-energy cross sections.

The paper is organized as follows. In Sec. II, we briefly present the three-cluster microscopic model and give the conditions of the calculation. Section III is devoted to spectroscopic properties of $^{21}$Ne and $^{21}$Na. In Sec. IV, we analyze the $^{17}O+\alpha$ and $^{20}Ne+n$ elastic phase shifts and the $^{17}O(\alpha,\gamma)^{21}Ne$ and $^{17}O(\alpha,n)^{20}Ne$ cross sections. Nuclear reaction rates are computed and compared to values currently employed in astrophysics. The $^{20}Ne(p,\gamma)^{21}Na$, $^{20}Ne(p,p')^{20}Ne(2^+)$, and $^{20}Ne(p,\alpha)^{17}F$ cross sections are discussed in Sec. V, and concluding remarks are given in Sec. VI.

## II. MICROSCOPIC THREE-CLUSTER MODEL

### A. Wave functions

The $^{21}$Ne wave functions are constructed from $^{16}$O and $\alpha$ internal wave functions, defined in the harmonic oscillator model, with an oscillator parameter $b = 1.62$ fm. Fully antisymmetrized 21-body wave functions are obtained from Slater determinants $\Phi_{\alpha,K}(\mathbf{R}_\alpha,\mathbf{R})$ and $\Phi_{n,K}(\mathbf{R}_n,\mathbf{R})$ corresponding to the coupling modes $(\alpha+^{16}O)+n$ and $(n+^{16}O)+\alpha$, respectively (see Fig. 1), and to a spin projection of the neutron equal to $K$. In the former coupling mode, $^{16}$O and $\alpha$ orbitals are centered at the extremities of $\mathbf{R}_\alpha$, whereas $\mathbf{R}$ describes the $^{20}Ne+n$ relative motion. In the latter coupling mode, the roles of neutron and $\alpha$ are exchanged. Because of antisymmetrization, both coupling modes are equivalent for

 

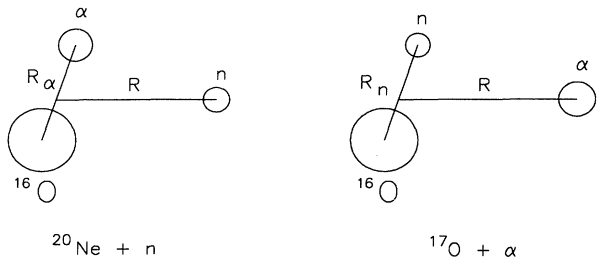


FIG. 1. $^{21}$Ne configurations.

small generator coordinates $\mathbf{R}_\alpha$, $\mathbf{R}_n$, and $\mathbf{R}$. However, the calculation of cross sections requires a correct treatment of boundary conditions. Accordingly, both coupling modes must be taken into account for a realistic description of scattering states. Using standard projection techniques [10], these Slater determinants are projected, first on $^{20}$Ne or $^{17}$O intrinsic spin $I_1$ and afterwards on total angular momentum $J$. In the GCM, total wave functions of $^{21}$Ne then read

$$\Psi^{JM\pi} = \sum_{I_1 I_\alpha \ell_\alpha} \sum_{R_\alpha, R} f^{J\pi}_{\alpha I_1 I_\alpha \ell_\alpha}(R_\alpha, R) \Phi^{JM\pi}_{\alpha I_1 I_\alpha \ell_\alpha}(R_\alpha, R) + \sum_{I_1 I_n \ell_n} \sum_{R_n, R} f^{J\pi}_{n I_1 I_n \ell_n}(R_n, R) \Phi^{JM\pi}_{n I_1 I_n \ell_n}(R_n, R), \quad (1)$$

where $\Phi^{JM\pi}$ basis functions are the projected Slater determinants and $f^{J\pi}$ the generator functions. In (1), $I_\alpha$ refers to the coupling of the $^{20}$Ne spin with an external neutron and $\ell_\alpha$ to the relative angular momentum. The index $n$ holds for the second coupling mode. The determination of the wave functions therefore relies on the calculation of the generator functions. These coefficients are obtained from the matrix elements of the Hamiltonian between projected Slater determinants. Owing to multiple angular momentum projection, this calculation involves five-dimensional integrals; it is outlined in Ref. [10].

### B. Conditions of the calculation

The $^{20}$Ne wave functions are defined with $R_\alpha = 2.9$ fm, which minimizes the $^{20}$Ne binding energy for the standard Volkov force V2 [12]. For $^{17}$O, we choose $R_n = 2.0$ fm which gives a satisfactory energy difference between the $\ell = 0$ and $\ell = 2$ states. In both cases, we restricted ourselves to a single generator coordinate since, owing to the angular momentum projection, computer times reach the limit of our current possibilities. In addition, a similar three-cluster approach of the $^{24}$Mg nucleus [13] shows that, provided the single generator coordinate is adequately chosen, the influence of additional values is rather small at low energies. Internal spins $I_1 = 0^+$, $2^+$, and $1^-$ are taken into account for $^{20}$Ne, and $I_1 = 5/2^+$, $1/2^+$, and $3/2^+$ for $^{17}$O and $^{17}$F. The adopted nucleon-nucleon force is the Volkov interaction V2 with a spin-orbit component [14]. The Majorana parameter $M$ and the spin-orbit strength $S_0$ are adjusted to reproduce the $^{21}$Ne ground-state energy with respect to the $^{20}$Ne+n threshold (−6.76 MeV) and the ($^{20}$Ne+$n$)−($^{17}$O+$\alpha$) energy difference (0.59 MeV). This yields $M = 0.6273$ and $S_0 = 25.25$ MeV fm$^5$.

TABLE I. Spectroscopic properties of $^{20}$Ne.

| | GCM | Expt.[a] |
|---|---|---|
| $E(2^+)$ (MeV) | 1.04 | 1.63 |
| $E(1^-)$ (MeV) | 7.91 | 5.78 |
| $\sqrt{\langle r^2 \rangle}(0^+)$ (fm) | 2.80 | 3.02 |
| $Q(2^+)$ ($e$ fm$^2$) | −11.8 | −20 ± 5 |
| $B(E2, 2^+ \to 0^+)$( $e^2$ fm$^4$) | 33.4 | 68 ± 4 |

[a]Ref. [15].

With these conditions, some spectroscopic properties of $^{20}$Ne, $^{17}$O, and $^{17}$F are given in Tables I and II. As it is well known [17], an $\alpha$+$^{16}$O description of $^{20}$Ne low-lying states underestimates deformation effects. This problem does not arise from the single generator coordinate limitation. For $^{17}$O and $^{17}$F, the GCM spectroscopic properties are in reasonable agreement with experiment, except for electric properties in $^{17}$O. The experimental values for $Q(5/2^+)$ and $B(E2, 1/2^+ \to 5/2^+)$ support core-polarization effects. These effects might be simulated by an effective charge, but since we are mainly concerned with $^{21}$Ne and $^{21}$Na wave functions, we do not include such effective charge here. The reliability of $^{17}$O wave functions is supported by the good r.m.s. and magnetic-moment values.

Let us now turn to the total 21-body wave functions. The relative generator coordinates $R$ relative to the $^{17}$O+$\alpha$ and $^{20}$Ne+$n$ motions are selected from 2.4 fm to 8.4 fm with a step of 1.2 fm. The matrix elements between projected Slater determinants are computed as explained in Ref. [10]. Scattering wave functions, collision matrices, and cross sections are determined in the microscopic $R$-matrix (MRM) method (see Refs. [17,18]).

## III. SPECTROSCOPIC PROPERTIES OF $^{21}$Ne AND $^{21}$Na

The $^{21}$Ne and $^{21}$Na spectra are presented in Fig. 2 for positive-parity states and in Fig. 3 for negative-parity states. Let us recall that all these states have been studied with the same nucleon-nucleon interaction. For the experimental data, we select, in the compilation of Endt [7], the states with a well defined spin assignment.

Let us first discuss $^{21}$Ne states. Below 6 MeV, there is almost no ambiguity to link experimental and GCM results. The $7/2^+$ (5629 keV) and $3/2^+$ (5822 keV) states in $^{21}$Ne have been suggested by Hoffmann *et al.* [5] to be "intruder" states which, in the shell-model theory, can be explained by multiple particle-hole excitations. In the present microscopic model, such phenomena are automatically included, except for excitation of the $^{16}$O core. The $7/2^+$ state is well explained by the GCM, but the $3/2^+$ "intruder" state should correspond to particle-hole

TABLE II. Spectroscopic properties of $^{17}$O and $^{17}$F.

| | $^{17}$O | | $^{17}$F | |
|---|---|---|---|---|
| | GCM | Expt.[a] | GCM | Expt.[a] |
| $E(1/2^+)$ (MeV) | 2.78 | 0.87 | 2.61 | 0.50 |
| $E(3/2^+)$ (MeV) | 5.77 | 5.08 | 5.77 | 5.82 |
| $\sqrt{\langle r^2\rangle}(5/2^+)$ (fm) | 2.58 | 2.67 | 2.58 | |
| $\mu(5/2^+)$ ($\mu_N$) | −1.90 | −1.89 | 4.79 | 4.72 |
| $Q(5/2^+)$ ($e$fm$^2$) | −0.03 | −2.58 | −6.4 | 10 ± 2 |
| $B(E2, 1/2^+ \to 5/2^+)$ ($e^2$fm$^4$) | 0.001 | 6.21 ± 0.08 | 26.1 | 64.9 ± 1.3 |

[a]Ref. [16].

excitations of $^{16}$O, which are not taken into account here. Such configurations might be simulated by using $^{15}$N or $^{14}$N cores, for instance, but the loss of the closed-shell structure of the core would require prohibitive computer times. The model suggests a $13/2^+$ excited state near $E_x$ = 7 MeV and a second $11/2^+$ state which might correspond to the 7.98 MeV or 8.24 MeV experimental levels.

Negative-parity states are given in Fig. 3. The GCM does not reproduce the three lowest states, which are known to be described by holes in the $p$ shell [5], and consequently would require an extension of our set of basis wave functions. In $^{21}$Ne, the model suggests a $1/2^-$ state near $E_x$=6.5 MeV, whose analog is observed in $^{21}$Na at $E_x$=4.98 MeV [7], but has not been observed yet in $^{21}$Ne.

In $^{21}$Na, it is interesting to point out that the first $1/2^+$ state has a rather strong experimental Coulomb shift (−0.37 MeV). Our calculation provides −0.20 MeV which indeed is much larger than for the other states. This Coulomb effect is due to the significant difference between the $^{20}$Ne+$n$ threshold energy in $^{21}$Ne and $^{20}$Ne+$p$ threshold energy in $^{21}$Na. Since the $1/2^+$ state is very close to the $^{20}$Ne+$p$ threshold (−7 keV), the behavior of the wave function at large distances is very different for $^{21}$Ne and $^{21}$Na. This weakly bound $1/2^+$ state plays an important role in the $^{20}$Ne$(p,\gamma)^{21}$Na capture reaction (see Sec. V). The GCM predicts a $11/2^+$ level analog to the well known $11/2^+$ state in $^{21}$Ne. This state should correspond to the 4.41 MeV experimental state in $^{21}$Na, which has no spin assignment [7].

Spectroscopic properties of the $3/2^+$ ground state and $5/2^+$ first excited state are given in Table III. Except for the ground-state quadrupole moment in $^{21}$Ne, the GCM is compatible with experiment, if one considers that the model does not contain free parameters such as effective charges. Since the GCM reproduces fairly well the absolute value of $\mu(5/2^+)$, it is reasonable to trust the theoretical signs which are experimentally unknown. We do not have any explanation for the huge experimental value of $Q(3/2^+)$ in $^{21}$Ne. Since the magnetic moment supports the validity of the GCM wave function, we think that this experimental value might be renormalized.

The $^{20}$Ne+$p$ threshold in $^{21}$Na is rather low (2.43 MeV), and therefore most of $^{21}$Na states are resonances, whose widths can be compared with GCM counterparts. This provides a good test of $^{21}$Na wave functions which, owing to the isospin symmetry, can be partly extended to $^{21}$Ne analog states. However, the particle width of a low-energy resonance is well known to be strongly affected by its precise location. Instead of total widths, we therefore compare, in Table IV, dimensionless proton reduced widths. The GCM values have been calculated according to the $R$-matrix method [18], and the experimental values are determined from the total widths [7]. Below 5 MeV, the GCM wave functions are confirmed to be fairly accurate. For the $7/2^-_1$ and $3/2^-_3$ states, however, the model overestimates the data by one order of magnitude. This indicates that, in negative parity, wave functions are more complex than in positive parity. To reach the quality of positive-parity wave functions, it is

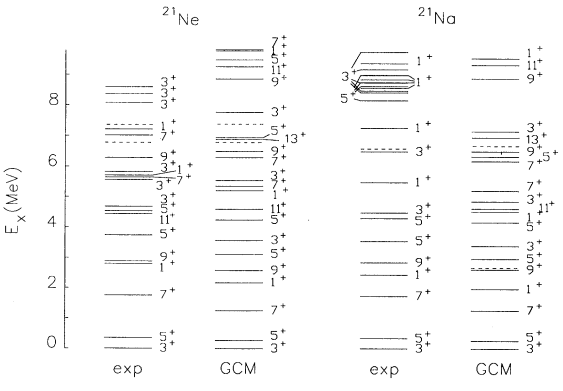


FIG. 2. Energy spectra for positive-parity states of $^{21}$Ne and $^{21}$Na. Experimental data are taken from Ref. [7]. The $\alpha$ and nucleon thresholds are represented by dashed lines (in the experimental $^{21}$Na spectrum, the $p$+$^{20}$Ne threshold and the energy of the $\frac{1}{2}^+_1$ state are almost identical).

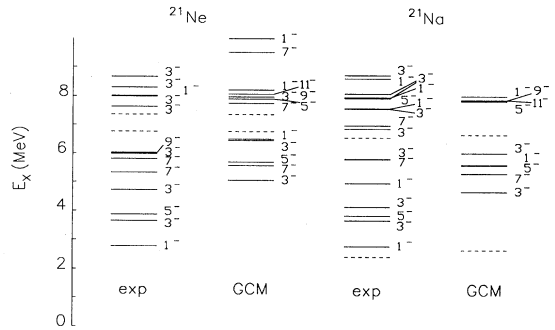


FIG. 3. See caption to Fig. 2 for negative-parity states.

TABLE III. Spectroscopic properties of $^{21}$Ne and $^{21}$Na low-lying states.

| | $^{21}$Ne | | $^{21}$Na | |
|---|---|---|---|---|
| | GCM | Expt.[a] | GCM | Expt.[a] |
| $Q(3/2^+)$ ($e$fm$^2$) | 8.2 | $-103 \pm 8$ | 10.3 | $5 \pm 4$ |
| $\mu(3/2^+)$ ($\mu_N$) | $-1.14$ | $-0.66$ | 2.93 | 2.39 |
| $Q(5/2^+)$ ($e$fm$^2$) | $-1.2$ | | | |
| $\mu(5/2^+)$ ($\mu_N$) | $-1.25$ | $\pm 0.53 \pm 0.07$ | 4.10 | $\pm 3.7 \pm 0.3$ |

[a]Ref. [7].

likely that core-excitation configurations should be added to the basis set.

A further test of GCM wave functions is provided by electromagnetic transition probabilities, displayed in Table V. Experimental data are deduced from Ref. [7] according to Ref. [4]. As for the previously studied properties, the experimental transition probabilities are fairly well reproduced by the GCM. Owing to the strong $B(E2)$ values between the $3/2^+_1$, $5/2^+_1$, $7/2^+_1$, $9/2^+_1$, and $11/2^+_1$ states, we confirm the existence of a $K^\pi = 3/2^+$ band involving these states [5].

## IV. $^{17}$O+$\alpha$ AND $^{20}$Ne+$n$ REACTIONS

### A. $^{17}$O($\alpha,\alpha$)$^{17}$O and $^{20}$Ne($n,n$)$^{20}$Ne elastic scattering

We present in Fig. 4 the GCM $^{17}$O+$\alpha$ elastic phase shifts. Hereafter, we use the notation $E^k_{\rm c.m.}$ for representing a c.m. energy with respect to the channel $k$. Negative-parity phase shifts are very small (less than 10°) in the considered energy range, and are therefore not shown here. In positive parity, the GCM phase shifts present a resonant structure, similar to that obtained in $^{16}$O+$\alpha$ scattering [19]. We find broad barrier resonances whose reduced width is close to the Wigner limit. For a channel radius equal to 8.4 fm, we have $\theta^2_\alpha = 13\%$ for $(\ell, J) = (0, 5/2^+)$, and $\theta^2_\alpha = 32\%$, 37%, 32%, 49%, and 25% for $\ell = 2$ and $J = 1/2^+$, $3/2^+$, $5/2^+$, $7/2^+$, and $9/2^+$, respectively. These resonances can therefore be interpreted as "molecular" states, with a marked $^{17}$O+$\alpha$ structure. This phenomenon is well known in $\alpha$ + nucleus systems [19].

Figure 5 illustrates $^{20}$Ne+$n$ elastic phase shifts. The

TABLE IV. Dimensionless reduced widths $\theta^2_p$ (at 8.4 fm) in $^{21}$Na. Energies are expressed in MeV, and reduced widths in %. Experimental data are taken from Ref. [7].

| $J^\pi$ | $E_x$ (Expt.) | $\theta^2_p$ (GCM) | $\theta^2_p$ (Expt.) |
|---|---|---|---|
| $5/2^+_2$ | 3.54 | 0.027 | 0.015 |
| $3/2^-_2$ | 3.68 | 9.9 | 12.6 |
| $5/2^+_3$ | 4.29 | 0.27 | 0.54 |
| $3/2^+_2$ | 4.47 | 2.0 | 2.2 |
| $1/2^-_2$ | 4.98 | 17.3 | 7.3 |
| $1/2^+_2$ | 5.46 | 14.6 | 2.7 |
| $7/2^-_1$ | 5.82 | 0.7 | $\approx 0.03$ |
| $3/2^-_3$ | 5.83 | 9.1 | 0.6 |

TABLE V. Electromagnetic transition probabilities (in W.u.) for different multipoles $\sigma\lambda$.

| | | | $^{21}$Ne | | $^{21}$Na |
|---|---|---|---|---|---|
| $J_i$ | $J_f$ | $\sigma\lambda$ | GCM | Expt.[a] | GCM |
| $1/2^+_1$ | $3/2^+_1$ | $M1$ | 1.2 | $0.20 \pm 0.03$ | 1.5 |
| $5/2^+_1$ | $3/2^+_1$ | $M1$ | 0.04 | $0.071 \pm 0.001$ | 0.06 |
| | | $E2$ | 14.4 | $24 \pm 3$ | 18.9 |
| $7/2^+_1$ | $3/2^+_1$ | $E2$ | 6.2 | $10.6 \pm 2.4$ | 9.5 |
| $7/2^+_1$ | $5/2^+_1$ | $M1$ | 0.06 | $0.16 \pm 0.02$ | 0.07 |
| | | $E2$ | 12.4 | $11.8 \pm 3.5$ | 16.9 |
| $9/2^+_1$ | $5/2^+_1$ | $E2$ | 11.3 | $16.2 \pm 2.5$ | 10.7 |
| $9/2^+_1$ | $7/2^+_1$ | $M1$ | 0.15 | $0.25 \pm 0.04$ | 0.19 |
| | | $E2$ | 9.1 | $9.6 \pm 5.0$ | 5.9 |
| $11/2^+_1$ | $7/2^+_1$ | $E2$ | 12.6 | $13.7 \pm 4.6$ | 14.7 |
| $11/2^+_1$ | $9/2^+_1$ | $M1$ | 0.16 | $0.21 \pm 0.06$ | 0.20 |
| | | $E2$ | 6.0 | $6.4 \pm 3.8$ | 7.1 |

[a]Ref. [7].

$1/2^+$ phase shift presents the well known $\sqrt{E}$ energy dependence. For $J^\pi = 3/2^+$, we find a narrow resonance ($\Gamma_n = 43$ keV) near $E^n_{\rm c.m} = 1$ MeV (see also Fig. 2). Experimental candidates are the 1.30 MeV or 1.60 MeV $3/2^+$ resonances whose widths ($8 \pm 3$ keV and $10 \pm 3$ keV) are comparable to the GCM ones. Because of the centrifugal barrier, phase shifts corresponding to higher angular momenta are negligible in this energy range. As it can be seen on the energy spectrum (Fig. 3), negative-parity phase shifts present narrow resonances near the threshold. The properties of the GCM $1/2^-$ resonance ($E^n_{\rm c.m} = 1.44$ MeV, $\Gamma_n = 125$ keV) suggest to link it with the experimental $1/2^-$ resonance at $E^n_{\rm c.m} = 1.24$ MeV ($\Gamma_n = 32 \pm 6$ keV). The width of the low-energy $3/2^-$ resonance is 180 keV; as shown in Fig. 3, there are several $3/2^-$ experimental states in this energy region, but no definite assignment can be done because of the similar neutron widths. There is no experimental counterpart for the GCM $5/2^-$, $7/2^-$, and $9/2^-$ resonances, but several states, without spin assignment, are experimentally observed near the neutron threshold, and might be related to the theoretical resonances. Other resonances are

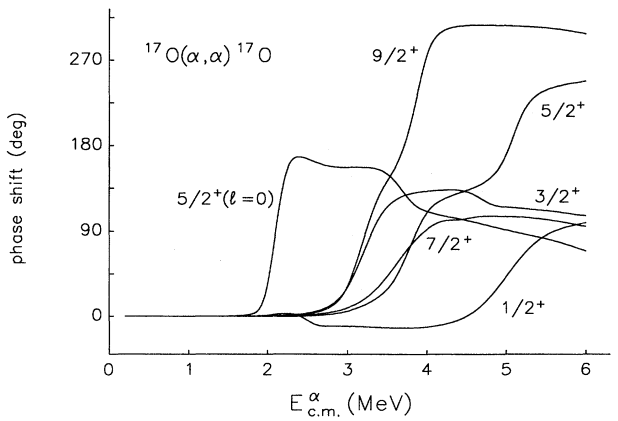


FIG. 4. $^{17}$O + $\alpha$ elastic phase shifts for $\ell = 0$ and $\ell = 2$. The curves are labeled by the total spin $J^\pi$.

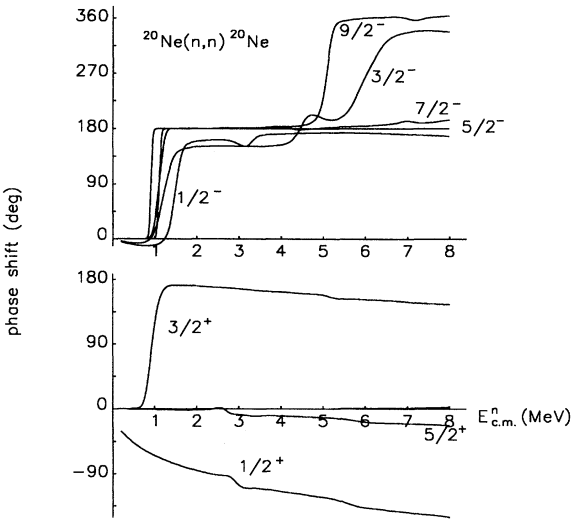


FIG. 5. $^{20}$Ne+$n$ elastic phase shifts. The curves are labeled by the total spin $J^\pi$.

predicted at higher energy, but experimental assignments are not possible.

### B. $^{17}$O($\alpha,\gamma$)$^{21}$Ne and $^{17}$O($\alpha$,$n$)$^{20}$Ne reactions

The $^{17}$O$(\alpha,\gamma)^{21}$Ne and $^{17}$O$(\alpha,n)^{20}$Ne reaction rates and, more especially, the ratio between them play an important role in some astrophysical scenarios [20]. However, the lack of experimental data makes the current estimates of reaction rates very uncertain [8]. In the present microscopic approach, we cannot hope to determine "definite" reaction rates, because the level density in $^{21}$Ne near the $^{17}$O+$\alpha$ threshold is rather high. However, the GCM energy spectrum, shown in Figs. 2 and 3, is fairly close to experiment, and should allow us to provide at least a rough estimate of the $^{17}$O+$\alpha$ reaction rates. In addition, these reaction rates are expected to be mostly given by the contribution of resonances with a marked $^{17}$O+$\alpha$ structure, which are well reproduced by our configuration choice.

In Fig. 6(a), we present the GCM $^{17}$O$(\alpha,\gamma)^{21}$Ne $S$ factors, where we include the $E1$, $E2$, and $M1$ multipolarities. The ground-state contribution turns out to be negligible in the considered energy range. Since most of the final $^{21}$Ne states have a positive parity, $E1$ transitions favor negative-parity initial partial waves. The capture cross section is affected by a $3/2^-$ resonance near 0.5 MeV, which corresponds to the lowest negative angular momentum ($\ell = 1$). For the sake of completeness, we have to remember that the three lowest negative-parity states of $^{21}$Ne are not reproduced by our model (see Fig. 3) and should therefore enlarge the capture cross section. However, since these states are not described by an $^{17}$O+$\alpha$ structure, their overlap with $^{17}$O+$\alpha$ scattering states should be small. It is therefore reasonable to expect a negligible contribution from these low-energy negative-parity states.

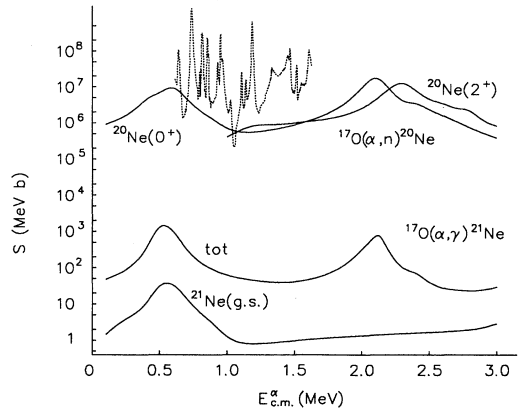


FIG. 6. $^{17}$O$(\alpha,\gamma)^{21}$Ne and $^{17}$O$(\alpha,n)^{20}$Ne $S$ factors. The dashed line represents the $^{17}$O$(\alpha,n)^{20}$Ne experimental data of Denker *et al.* [21].

Figure 6(b) shows the GCM $^{17}$O$(\alpha,n)^{20}$Ne $S$ factor. Since the energy dependence is given by initial $^{17}$O+$\alpha$ scattering wave functions, it greatly resembles the energy dependence of the $^{17}$O$(\alpha,\gamma)^{21}$Ne $S$ factor. We display as dotted lines the recent experimental data of the Stuttgard group [21]. These data exhibit many narrow resonances which, owing to the large excitation energy in the $^{21}$Ne compound nucleus, are missing here. However, if one removes these narrow resonances, the remaining background contribution is fairly close to the GCM result. We can therefore expect that our low-energy $S$ factor is a realistic estimate of the nonresonant part. We also present the contribution of the $^{20}$Ne($2^+$) first excited state. Since the theoretical excitation energy of the $2^+$ state is slightly too small (see Table I), the GCM contribution below the experimental threshold 1.63 MeV should be disregarded. However, as long as we are interested in orders of magnitude only, this does not affect our conclusions. In addition, the $^{20}$Ne($2^+$) contribution vanishes in the astrophysical domain.

In Fig. 7, we give the $^{17}$O$(\alpha,\gamma)^{21}$Ne and $^{17}$O$(\alpha,n)^{20}$Ne reaction rates as a function of temperature. These reac-

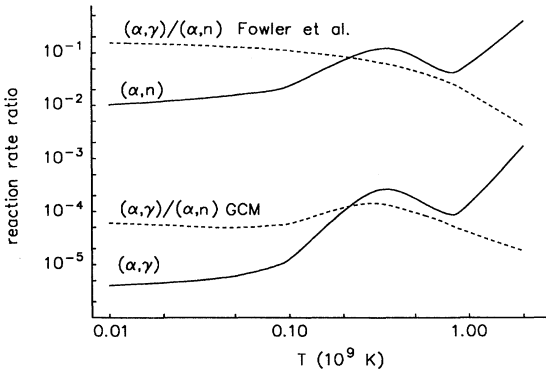


FIG. 7. Ratios of the present $(\alpha,\gamma)$ and $(\alpha,n)$ reaction rates with the values of Caughlan and Fowler [8] (solid lines). The $(\alpha,\gamma)/(\alpha,n)$ ratios are plotted as dashed lines. Temperatures are expressed in $10^9$ K.

tion rates have been obtained by numerical integration of the GCM cross section times the Maxwell-Boltzmann distribution. In place of the absolute values, we present the GCM reaction rates with respect to the compilation of Caughlan and Fowler [8]. For the $(\alpha, n)$ reaction, we find a reaction rate lower by 1 or 2 orders of magnitude, but the difference with the compilation of Caughlan and Fowler is much larger for the $(\alpha, \gamma)$ reaction (4–5 orders of magnitude). This result strongly affects the $(\alpha, \gamma)/(\alpha, n)$ ratio which is expected to be characteristic of the ratio between the electromagnetic and nuclear forces. Our value, close to $10^{-4}$ in the whole temperature range, should significantly affect the $s$-process nucleosynthesis in massive stars [20]. Of course, the present $(\alpha, \gamma)$ and $(\alpha, n)$ reaction rates might be enhanced by some missing resonances, but we think that this problem should weakly modify the GCM $(\alpha, \gamma)/(\alpha, n)$ ratio.

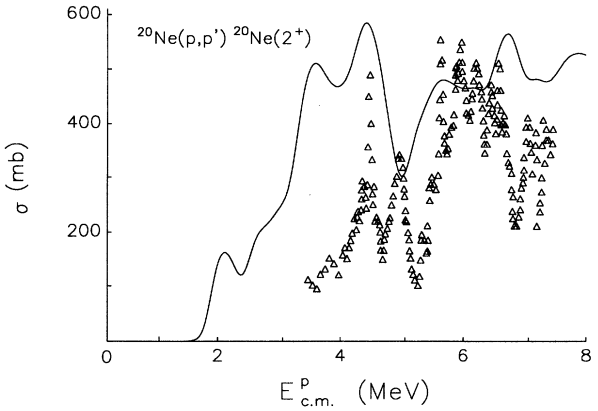


FIG. 9. $^{20}$Ne$(p, p')^{20}$Ne$(2^+)$ cross section; experimental data are taken from Ref. [22].

## V. $^{20}$Ne$(p,\gamma)^{21}$Na AND $^{20}$Ne$(p,\alpha)^{17}$F REACTIONS

The $^{20}$Ne$(p,\gamma)^{21}$Na reaction is the starting point of the Ne-Na cycle [6] which is important for nucleosynthesis of heavy elements in massive stars. The capture cross section has been measured by Rolfs *et al.* [6] down to 350 keV, but the astrophysical energies are still lower (< 100 keV) and the corresponding cross sections drop to very small values, unreachable in current experiments. At very low energies, the $^{20}$Ne$(p,\gamma)^{21}$Na cross section is expected to be dominated by the contribution of the $1/2^+$ (2.425 MeV) state in $^{21}$Na, which is bound by 7 keV only [6]. This subthreshold-state effect is well known in the $^{12}$C$(\alpha,\gamma)^{16}$O reaction, for example, and is responsible for a strong enhancement of the $S$ factor at low energies. However, this effect usually occurs below the lower limit of experiments, and its contribution must be estimated by extrapolation of the data.

We present in Fig. 8 the GCM $S$ factors, involving the $E1$, $E2$, and $M1$ multipolarities. The Majorana parameter of the $1/2^+$ weakly bound state has been slightly modified (0.6405 in place of 0.6273 throughout the paper) in order to exactly reproduce its binding energy (7 keV) with respect to the proton threshold. Figure 8 shows that the contribution of the $5/2^+$ first excited state is in good agreement with experiment. Capture to the $1/2^+$ state is underestimated, but the energy dependence of the $S$ factor is supported by the data. It should be pointed out that the underestimation problem is consistent with most theoretical studies of the spectroscopic factor [6]. The value deduced by Rolfs *et al.* from their data is significantly larger than spectroscopic factors quoted in the literature. As expected by Rolfs *et al.*, the ground-state contribution is strongly affected, at low energies, by the tail of the $1/2^+$ subthreshold state. Our $S$ factor is consistent with the data for the lowest energies. Beyond 1 MeV, the GCM $S$ factor is affected by resonances whose energies are not exactly reproduced and which therefore should be disregarded. In the astrophysical region ($E \leq$ 100 keV), the present $S$ factor is similar to the extrapolation of Rolfs *et al.*, and therefore does not change current estimates of the $^{20}$Ne$(p,\gamma)^{21}$Na reaction rate.

The $^{20}$Ne$(p,p')^{20}$Ne $(2^+)$ and $^{20}$Ne$(p,\alpha)^{17}$F cross sections, presented in Fig. 9 and Fig. 10, respectively, are valuable tests of the model. The order of magnitude of

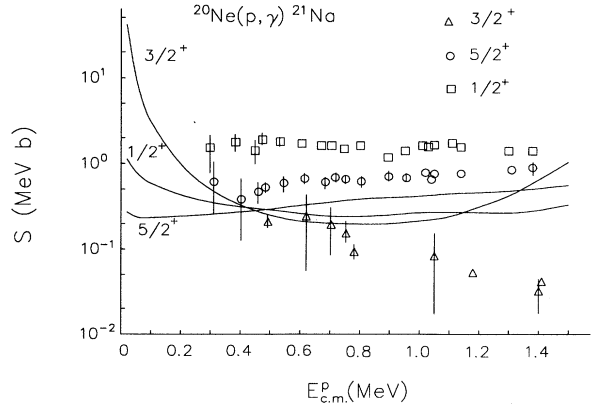


FIG. 8. $^{20}$Ne$(p,\gamma)^{21}$Na $S$ factors for the three bound states of $^{21}$Na. Experimental data are taken from Ref. [6].

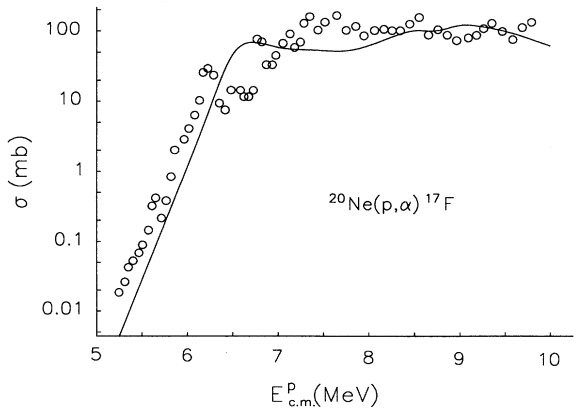


FIG. 10. $^{20}$Ne$(p,\alpha)^{17}$F cross section; experimental data are taken from Ref. [23].

the $^{20}$Ne$(p,p')^{20}$Ne$(2^+)$ cross section is consistent with the data of Fernandez *et al.* [22], but the apparent energy shift between GCM and experiment is mainly due to a threshold effect. The GCM calculation gives, for the $2^+$ state in $^{20}$Ne, $E_x = 1.04$ MeV (see Table I) whereas the experimental value is $E_x = 1.63$ MeV. Consequently, the microscopic cross section starts rising at energies lower than in experiment. For the $^{20}$Ne$(p,\alpha)^{17}$F transfer cross section, presented in Fig. 10, we obtain a fair agreement with the experimental data of Gruhle and Kober [23]. This is an indication of the reliability of the coupling strength between the $^{20}$Ne$+p$ and $^{17}$F$+\alpha$ configurations.

## VI. CONCLUSION

This work aims at reviewing different properties of the 21-nucleon $T = \frac{1}{2}$ systems, in a microscopic framework. The present three-cluster model involves $^{16}$O and $\alpha$ wave functions which are well described by the harmonic oscillator model. Accordingly, $^{21}$Ne and $^{21}$Na wave functions, defined by mixing of $^{16}$O$+\alpha+n$ or $^{16}$O$+\alpha+p$ configurations, are expected to be realistic. We have tested these wave functions by computing several well known quantities, such as energy spectra or electromagnetic transition probabilities. Of course, one cannot hope to get a perfect description of all properties, but the overall agreement can be considered as good for systems such as $^{21}$Ne or $^{21}$Na. These rather heavy systems are close to the limit of microscopic models, where all nucleons are taken into account and where the Pauli principle is treated exactly.

The GCM $^{17}$O$(\alpha,n)^{20}$Ne cross section is compatible with the recent data of the Stuttgart group [21], and provides a reaction rate lower than the estimate of Caughlan and Fowler [8] by 2 orders of magnitude. An even stronger difference is obtained for the $^{17}$O$(\alpha,\gamma)^{21}$Ne reaction rate which is lower by more than 5 orders of magnitude in a wide temperature range. Even if the present calculation cannot be considered as the "final" result, we think that the difference is significant and that the present $(\alpha,\gamma)/(\alpha,n)$ branching ratio should be important in some astrophysical applications [20]. For the $^{20}$Ne$(p,\gamma)^{21}$Na reaction, we do not predict modifications with respect to the reaction rate used in astrophysics.

The present description of 21-nucleon systems might be improved by taking account of other configurations, either with $^{16}$O excited states or with cores different from $^{16}$O. This should mainly improve the negative-parity wave functions and provide the lowest negative-parity states which are missing here. A second improvement would be the introduction of distortion effects in $^{20}$Ne and $^{17}$O (or $^{17}$F) through the use of several $R_\alpha$ or $R_n$ [see Eq. (1)] generator coordinates. However, the present three-cluster model requires large computer times, owing to the double projection on $^{20}$Ne or $^{17}$O and on the total $^{21}$Ne spins. Going beyond our assumptions would increase the computer times by orders of magnitude. We think that the present description is satisfactory and that a better knowledge of 21-nucleon systems does not deserve such a tremendous effort.

## ACKNOWLEDGMENTS

I am grateful to Dr. A. Denker for interesting discussions concerning the $^{17}$O$(\alpha,n)^{20}$Ne reaction. This work was supported by the Fonds National de la Recherche Scientifique. The numerical calculations have been carried out thanks to a supercomputer grant on the CRAY Y-MP of the ULB computer center.

[1] C. Rolfs, E. Kuhlmann, F. Riess, and R. Kraemer, Nucl. Phys. **A167**, 449 (1971).
[2] C. Rolfs, H.P. Trautvetter, E. Kuhlmann, and F. Riess, Nucl. Phys. **A189**, 641 (1972).
[3] E. Kuhlmann, A. Hoffmann, and W. Albrecht, Z. Phys. A **271**, 281 (1974).
[4] G. Andritsopoulos, W.N. Catford, E.F. Garmann, D.M. Pringle, and L.K. Fifield, Nucl. Phys. **A372**, 281 (1981).
[5] A. Hoffmann, P. Betz, H. Röpke, and B.H. Wildenthal, Z. Phys. A **332**, 289 (1989).
[6] C. Rolfs, W.S. Rodney, M.H. Shapiro, and H. Winkler, Nucl. Phys. **A241**, 460 (1975).
[7] P.M. Endt, Nucl. Phys. **A521**, 1 (1990).
[8] G. R. Caughlan and W. A. Fowler, At. Data Nucl. Data Tables **40**, 283 (1988).
[9] P. Descouvemont, J. Phys. G **19**, S141 (1993).
[10] D. Baye and P. Descouvemont, in *Proceedings of the International Symposium on Developments of Nuclear Cluster Dynamics,* Sapporo, Japan, 1988, edited by Y. Akaishi *et al.* (World Scientific, Singapore, 1989), p. 6.
[11] P. Descouvemont and D. Baye, Nucl. Phys. **A517**, 143 (1990).
[12] A.B. Volkov, Nucl. Phys. **74**, 33 (1965).
[13] P. Descouvemont and D. Baye, Phys. Lett. B **228**, 6 (1989).
[14] D. Baye and N. Pecher, Bull. Cl. Sci. Acad. R. Belg. **67**, 835 (1981).
[15] F. Ajzenberg-Selove, Nucl. Phys. **A475**, 1 (1987).
[16] F. Ajzenberg-Selove, Nucl. Phys. **A460**, 1 (1986).
[17] D. Baye and P. Descouvemont, Nucl. Phys. **A407**, 77 (1983).
[18] P. Descouvemont and M. Vincke, Phys. Rev. A **42**, 3835 (1990).
[19] Y. Fujiwara, H. Horiuchi, K. Ikeda, M. Kamimura, K. Katō, Y. Suzuki, and E. Uegaki, Prog. Theor. Phys. Suppl. **68**, 29 (1980).
[20] I. Baraffe and K. Takahashi, Astron. Astrophys. (submitted).
[21] A. Denker *et al.*, in Proceedings of the 7th Workshop of Ringberg, MPA, 1993 (in press).
[22] M. Fernandez, G. Murillo, J. Ramirez, O. Avila, S.E. Darden, M.C. Rozak, J.L. Foster, B.P. Hichwa, and P.L. Jolivette, Nucl. Phys. **A369**, 425 (1981).
[23] W. Gruhle and B. Kober, Nucl. Phys. **A286**, 523 (1977).